Journal of Sound and Vibration (2001) **239**(1), 1–17
doi:10.1006/jsvi.2000.3114, available online at http://www.idealibrary.com on IDEAL®

PASSAGE THROUGH RESONANCE OF ROLLING FINNED PROJECTILES WITH CENTER-OF-MASS OFFSET

A. Sharma and N. Ananthkrishnan

Department of Aerospace Engineering, Indian Institute of Technology, Bombay, Powai, Mumbai 400076, *India. E-mail: akn@aero.iitb.ernet.in*

(*Received* 23 *June* 1999, *and in final form* 18 *April* 2000)

Finned projectiles that are meant to be unspun could acquire small roll rates in flight due to slight configurational asymmetries. If the roll rate matches the natural yawing frequency of the projectile, a resonance phenomenon takes place resulting in yaw amplification, and possible loss of stability. To avoid this, finned projectiles are deliberately spun to a roll rate well beyond the resonance value. This gives rise to a passage-through-resonance phenomenon in the flight of finned projectiles. Finned projectiles passing through resonance are known to exhibit the phenomena of roll lock-in, transient resonance, and catastrophic yaw. Projectiles locked in at the resonance condition experience large yaw and are likely to lose the desired flight path. On the other hand, transient resonance is a milder phenomenon where the projectile locks in at resonance briefly before continuing to build-up to the design value. However, the yaw amplification during the brief period of resonance may be sufficient to destabilize the projectile. The problem of passage through resonance of finned projectiles with a center-of-mass offset is considered in this paper. Roll lock-in and transient resonance at normal and reverse resonance is shown. It is observed that the yaw amplification at transient resonance is much lower than that at lock-in. The lack of yaw amplification can be understood based on the bifurcation analysis and numerical simulations reported in this paper.

1. INTRODUCTION

Antitank kinetic energy projectiles are designed to engage their targets at high speeds. These projectiles typically follow a horizontal, approximately straight line, trajectory with flight times of a few seconds. For maximum impact, they are launched with high muzzle velocities, and are intended to fly without spinning and with no yaw. Static stability is achieved by the use of fins instead of the common practice of spin stabilization, while the desired zero-yaw trajectory ensures minimum aerodynamic drag. These measures are meant to minimize the bleed during the flight of the kinetic energy at launch. The fins also provide yaw damping to damp out the precessional and nutational motion in case such a projectile experiences a yaw disturbance in flight. Properly designed fins can therefore provide both static and dynamic stability without the need for spinning the projectile.

In practice, finned projectile trajectories can deviate from the ideal flight described above due to configurational asymmetries. These arise from damage to the fins during launch or flight, or due to manufacturing tolerance [1]. Slight configurational asymmetries cause the projectile to trim at a non-zero value of yaw, and may set the projectile into a rolling or spinning motion. A small trim angle causes no harm by itself except for an increase in drag, but the small roll rate can easily match with the frequency of nutational motion causing a phenomenon called roll resonance or roll–yaw resonance. A projectile in flight undergoing

0022-460X/01/010001 + 17 $35.00/0

roll resonance, experiences an amplification of the trim angle resulting in large-amplitude yawing motion, which may cause instability.

The common solution to avoid roll resonance is to use canted fins. On launch, the canted fins create a rolling moment that rolls the projectile through the resonance region to a sufficiently large roll rate. Thus, as the projectile is spun up to the design roll rate in flight, the dynamics in roll experiences a passage-through-resonance phenomenon. While some amplification in yaw is to be expected during passage through resonance, in some instances, the roll rate is seen to lock in at the resonance frequency resulting in large-amplitude yawing motion, and loss of stability. This phenomenon has been called roll lock-in, roll–yaw lock-in or spin–yaw lock-in. In other cases, the roll rate may linger for a while at the resonance condition before eventually building up to the design value. This is a phenomenon called transient resonance. If transient resonance persists over a significant part of the flight trajectory, there is a possibility of trim angle amplification and yaw instability, even though roll lock-in *per se* does not actually occur. Another phenomenon is that of catastrophic yaw where the roll rate is locked into an oscillation about the resonance frequency while the yaw amplitude builds up to larger values than that during roll lock-in. Catastrophic yaw invariably leads to loss of stability and destruction of the projectile.

Thus, the problem of passage through resonance of rolling finned projectiles shows a whole host of interesting phenomena. Prediction of these phenomena requires the modelling and analysis of the dynamic equations for the flight of these projectiles.

1.1. REVIEW OF PREVIOUS WORK

A linear model for the yawing motion of projectiles, referred to as the linear aeroballistic theory [2], is capable of predicting the occurrence of roll resonance and the amplification of the trim angle at resonance. However, as the phenomena of roll lock-in, transient resonance, and catastrophic yaw in the passage-through-resonance problem of finned projectiles are non-linear in nature, linear aeroballistic theory is incapable of predicting such phenomena. Instead, a non-linear model for the coupled roll–yaw dynamics of the projectile flight is necessary.

The first attempt at modelling roll lock-in of finned projectiles was made by Nicolaides [3] who attributed the phenomenon to non-linear roll moments induced by the trim angle under resonance conditions. The primary cause of these induced roll moments was suggested by Price [4] to be an offset center of mass. The equations of motion for a finned projectile with an offset center of mass were formulated by Murphy [5], who showed that both normal and reverse roll lock-in was possible. Murphy [5] considered a non-linear induced roll moment due to the center-of-mass offset, but assumed the aerodynamic forces and moments to be linear. Minor corrections to the equations reported by Murphy [5] were carried out by Ananthkrishnan and Raisinghani [6], who also showed the possibility of occurrence of quasisteady roll lock-in. A detailed review of the theory of resonant lock-in of rolling finned projectiles with illustrative calculations has been provided by Ananthkrishnan and Raisinghani [7]. Dynamic instabilities of missiles and re-entry vehicles, including roll lock-in, have been reviewed in the papers by Murphy [8] and Platus [9]. A recent paper by Platus [10] discusses the problem in the context of coning instabilities in missiles and spacecraft.

The problem of transient resonance in finned projectiles was not investigated in either of references [5, 6]. Transient resonance in missiles with an offset center of mass had earlier been studied numerically by Price [4], and Barbera [11], and in the case of a non-linear induced roll moment of aerodynamic origin, by Chadwick [12]. The question of whether large yaw can be created due to trim amplification during transient resonance has yet to be

answered. Neither reference [5] nor reference [6] could demonstrate the phenomenon of catastrophic yaw, although reference [6] did point out that quasisteady solutions were possible where the roll rate could oscillate about the resonance frequency while the yaw showed an unlimited build-up. In fact, the model in reference [6] needs to be extended to include non-linear side forces and yawing moments in order to predict catastrophic yaw. At present, the model of reference [6] can be used to study roll lock-in and transient resonance.

All of the previous work cited above were based on numerical simulations to investigate the dynamic behavior of rolling finned projectiles in flight. Bifurcation analysis is a useful tool for studying the various phenomena in the passage-through-resonance problem of finned projectiles. In the present paper, the coupled roll–yaw dynamics of finned projectiles with an offset center of mass as given in reference [6] is analyzed by bifurcation methods. The AUTO continuation algorithm of Doedel *et al.* [13] is used for carrying out the bifurcation analysis. Stable normal and reverse resonant lock-in solutions are found to originate at saddle-node bifurcation points. Changes in the stability of the lock-in and design solutions with varying flight and projectile parameters are investigated. Numerical simulations are used to supplement the results from the bifurcation analysis. Passage through normal and reverse resonance is studied, and the effect of transient resonance on the trim amplification is evaluated, throwing new light on the passage through resonance phenomenon. The conclusions of this study have potential application to other problems of passage through resonance, see for example, reference [14].

2. EQUATIONS OF MOTION

The equations of motion for the flight of a finned projectile are written in an aeroballistic axis system. The aeroballistic axis system is a non-rolling reference frame in that the aeroballistic axes do not roll with the projectile but they pitch and yaw with the projectile, just as any other body-fixed axis system [7]. The coupled roll–yaw dynamic equations, as given in reference [6], appear as follows, where the overdots indicate derivatives with respect to dimensionless time t_1.

$$\ddot{\phi} + \hat{K}_p[\dot{\phi} - \dot{\phi}_s - \mathrm{i}G(\mu - \bar{\mu})] = 0, \tag{1}$$

$$\ddot{\mu} + [\hat{H} + \mathrm{i}(2-\sigma)\dot{\phi}]\dot{\mu} + [(1-\sigma)(1 - \dot{\phi}^2 + \mathrm{i}\dot{\phi}h) + \mathrm{i}\ddot{\phi}]\mu = -h(1-\sigma)\mathrm{e}^{\mathrm{i}\phi_M}. \tag{2}$$

The derivation of these equations is available in reference [15].

Equation (1) is a first order equation for the roll dynamics, where $\dot{\phi}$ is a scaled roll rate, such that $\dot{\phi} = \pm 1$ at resonance. Equation (2) is a second-order equation for the yaw dynamics, where μ is the complex angle of attack in the missile-fixed frame scaled with respect to the trim angle magnitude at resonance. Thus, equations (1) and (2) represent a set of five first order differential equations for the coupled roll-yaw dynamics. In the above equations, h represents the trim asymmetry with orientation ϕ_M, G is a measure of the center-of-mass offset, K_p and $\hat{H}$ represent the damping in the roll and yaw dynamics, respectively, and σ is the ratio of the roll to yaw moments of inertia.

2.1. EQUILIBRIUM SOLUTIONS

Equilibrium solutions of equations (1) and (2) are given by

$$\dot{\phi}_e = \dot{\phi}_s + \mathrm{i}G(\mu_e - \bar{\mu}_e), \tag{3}$$

$$\mu_e = -h(1 - \dot{\phi}_e^2 + \mathrm{i}\dot{\phi}_e h)^{-1}\mathrm{e}^{\mathrm{i}\phi_M}. \tag{4}$$

The equilibrium solutions depend on the parameters $\dot{\phi}_s$, h, ϕ_M and G. Among these, values of $\dot{\phi}_s$ and h are maintained constant at $\dot{\phi}_s = 3$ and $h = 0{\cdot}1$, while equilibrium roll rates with varying G for values of $\phi_M = 0$, 90, 180 and 270° are plotted in Figure 1(a–d). The other parameters, $\hat{H}$, $\hat{K}_p$, σ, influence the stability of these equilibrium points and are kept constant at $\hat{H} = 0{\cdot}1$, $\hat{K}_p = 0{\cdot}1$, and $\sigma = 0{\cdot}1$ for the computations in Figure 1. Stable solutions in Figure 1 are indicated by a full line and unstable solutions by a dashed line. Cases (a) and (b) show stable normal lock-in solutions for $\dot{\phi} \approx +1$, while

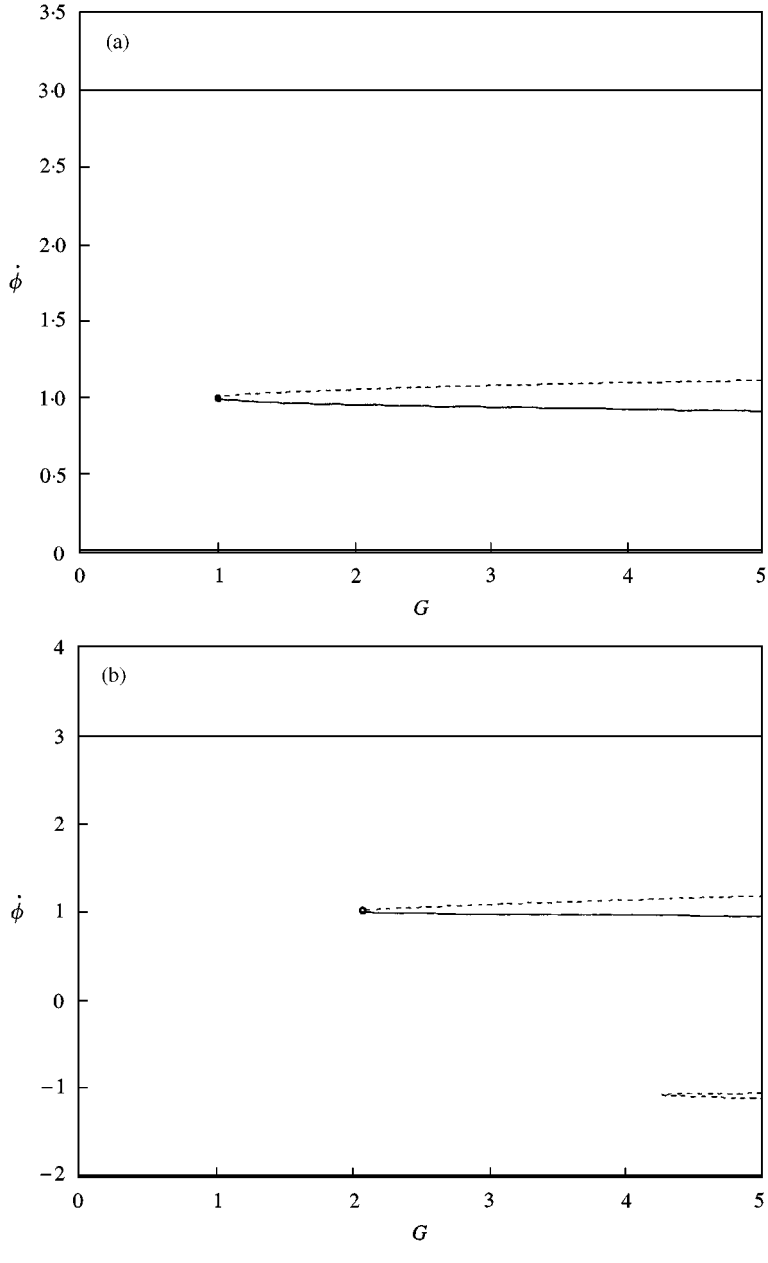

Figure 1. Equilibrium roll rates with varying G for (a) $\phi_M = 0°$, (b) $\phi_M = 90°$, (c) $\phi_M = 180°$, and (d) $\phi_M = 270°$: ——, stable equilibria; ----, unstable equilibria; ○○○, saddle-node bifurcation points).

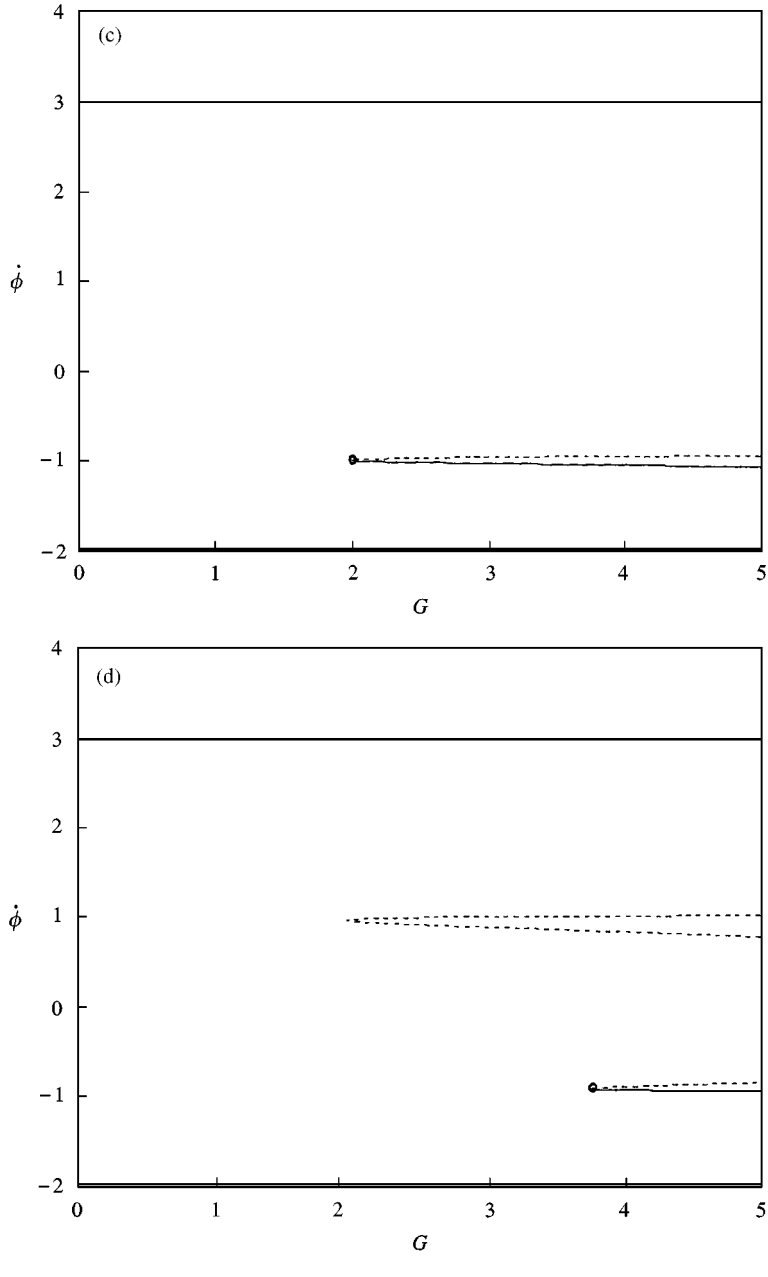

Figure 1. Continued.

cases (c) and (d) show stable reverse lock-in solutions for $\dot{\phi} \approx -1$. The design solution $\dot{\phi} \approx 3$ is stable in all four cases.

Two interesting observations can be made from the plots in Figure 1. Firstly, it is seen that for a given value of ϕ_M, there is a minimum value of G above which stable lock-in solutions occur. Secondly, stable lock-in solutions are seen to be created at the saddle-node bifurcation points [16], and are paired with an unstable solution with roll rate very near the lock-in roll rate. These unstable solutions will be seen to play an important role in the problem of passage through resonance.

2.2. NUMERICAL SIMULATIONS

Figure 1 shows that multiple stable equilibrium solutions are possible for several combinations of G and ϕ_M. For example, Table 1 lists all the equilibrium solutions for two cases out of all the possibilities indicated in Figure 1. Case A for $G = 5$, $\phi_M = 90^\circ$ shows a stable normal lock-in solution and a stable design solution, while Case B for $G = 5$, $\phi_M = 270^\circ$ shows a stable reverse lock-in solution and a stable design solution. Thus, cases A and B in Table 1 show two stable equilibrium solutions each. Which of the two stable equilibrium solutions is attained depends on the initial conditions at launch. The effect of disturbances at launch is given naturally in terms of initial conditions on the yaw rate, with the complex angle of attack and roll rate assumed to be zero initially. These two cases in Table 1 will be used to illustrate the results in the rest of this paper.

In order to evaluate the probability of occurrence of the normal and reverse lock-in solutions, numerical simulations are carried out with a matrix of 16 initial conditions of yaw rate spanning a range of amplitudes and orientations of the initial disturbance. The steady state attained for each of this set of 16 initial conditions for cases A and B is tabulated in Table 2, where *SD*, *SN*, and *SR* refer to the stable equilibrium states listed in Table 1. It is seen that 10 of the 16 initial conditions in case A end up at the normal lock-in steady state, while only 1 of the 16 results in reverse lock-in in case B. Similar results can be observed for other combinations of ϕ_M and G. Thus, it may be concluded that in case both normal lock-in and design solutions are stable, the occurrence of normal lock-in is highly likely. On the other hand, between stable reverse lock-in and stable design solution, the probability of occurrence of stable reverse lock-in is very low.

Results of some of the simulations in Table 2 illustrating the passage through resonance to the design solution, and lock-in at normal and reverse resonance are shown in Figures 2–4. Figure 2 shows simulation no. 13 for case A where the roll rate passes through resonance and builds up to the design value while the magnitude of the complex angle of attack dies to zero. According to the linear aeroballistic theory, the complex angle of attack consists of three modes: nutation, precession, and trim. Stable dynamics implies that, at steady state, the nutation and precession modes will have damped out, and the complex angle of attack is precisely due to the trim component. However, in the transient phase before attainment of steady state, all the three modes contribute to the yaw dynamics. The

TABLE 1

Equilibrium solutions and their stability

$\dot{\phi}_e$	β_e	α_e	Stability
Case A: $G = 5$, $\phi_M = 90^\circ$			
− 1·0857	0·2481	0.4086	Unstable (U)
− 1·0268	0·7607	0·4027	Unstable (U)
1·0106	− 0·9478	0·1989	Stable-normal Lock-in (SN)
1·2410	− 0·0404	0·1759	Unstable (U)
2·8611	− 0·0006	0·0139	Stable-design (SD)
Case B: $G = 5$, $\phi_M = 270^\circ$			
− 0·9765	− 0·8347	0·3976	Stable-reverse Lock-in (SR)
− 0·8816	− 0·1536	0·3882	Unstable (U)
0·7536	0·0392	0·2246	Unstable (U)
0·9897	0·9687	0·2010	Unstable (U)
3·1148	0·0004	− 0·0115	Stable-design (SD)

TABLE 2

Steady state solutions for test initial conditions

Simulation no.	Initial yaw rate, $\dot{\mu}_0$	Case A	Case B
1	$0{\cdot}1 + 0i$	SD	SD
2	$0{\cdot}2 + 0i$	SD	SD
3	$0{\cdot}5 + 0i$	SD	SD
4	$1{\cdot}0 + 0i$	SD	SD
5	$0 + 0{\cdot}1i$	SN	SD
6	$0 + 0{\cdot}2i$	SN	SD
7	$0 + 0{\cdot}5i$	SN	SD
8	$0 + 1{\cdot}0i$	SD	SR
9	$-0{\cdot}1 + 0i$	SN	SD
10	$-0{\cdot}2 + 0i$	SN	SD
11	$-0{\cdot}5 + 0i$	SN	SD
12	$-1{\cdot}0 + 0i$	SN	SD
13	$0 - 0{\cdot}1i$	SD	SD
14	$0 - 0{\cdot}2i$	SN	SD
15	$0 - 0{\cdot}5i$	SN	SD
16	$0 - 1{\cdot}0i$	SN	SD

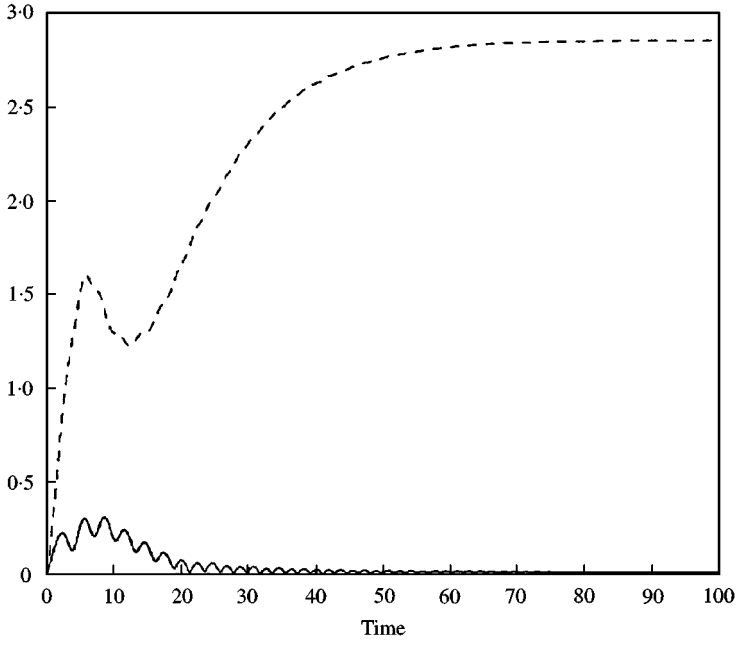

Figure 2. Variation of roll rate $\dot{\phi}$ (----), and magnitude of complex angle of attack $|\mu|$ (——) for simulation No. 13, case A in Table 2.

initial build-up of the complex angle of attack magnitude in Figure 2 is mainly due to the effect of the initial condition on the precession and nutation modes, and not because of trim amplification. Figure 3 shows the roll rate locking in at normal resonance in simulation no. 5 for case A. The initial yaw build-up is due to nutation and precession modes and is similar

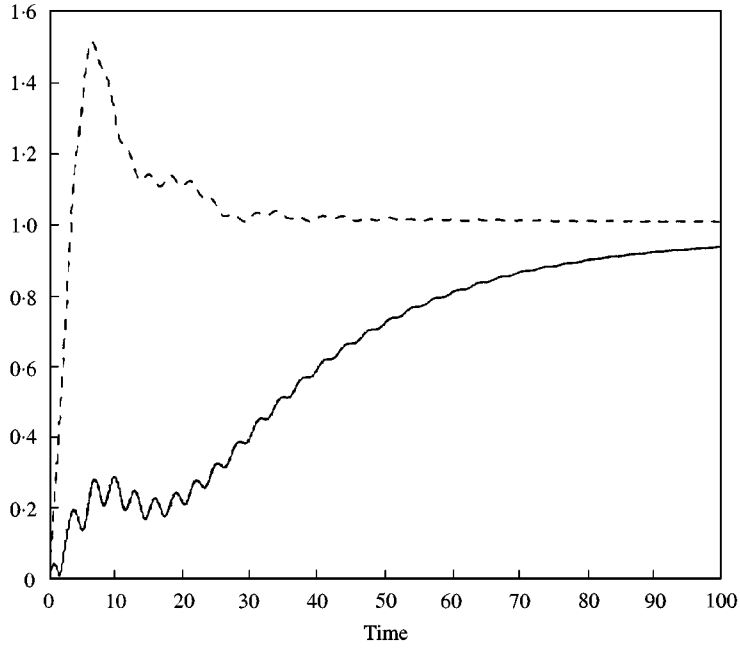

Figure 3. Variation of roll rate $\dot{\phi}$ (----), and magnitude of complex angle of attack $|\mu|$ (——) for simulation no. 5, case A in Table 2.

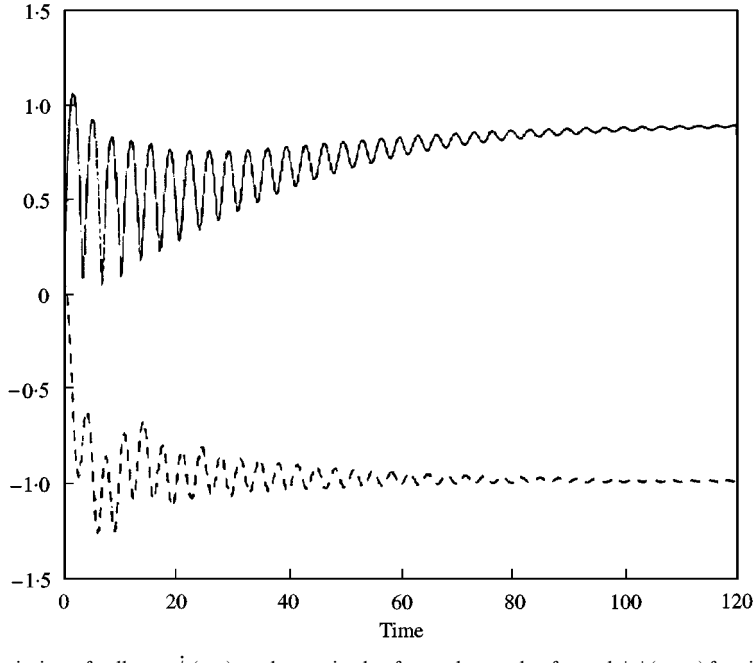

Figure 4. Variation of roll rate $\dot{\phi}$ (----), and magnitude of complex angle of attack $|\mu|$ (——) for simulation no. 8, case B in Table 2.

to that in Figure 2. However, even as these modes begin to die down, the complex angle of attack starts increasing around *time* = 20, corresponding to the roll rate locking in at normal resonance. This increase is due to the trim mode. At steady state, the complex angle of attack reaches the value given in Table 1. Figure 4 shows reverse lock-in in simulation

no. 8 for case B. The build-up in the complex angle of attack occurs in a similar fashion to that in Figure 3.

3. TRANSIENT RESONANCE

The test initial conditions in Table 2 have been listed in four groups based on the orientation of the initial yaw rate. Consider the second group of test initial conditions consisting of simulation nos. 5–8 for case A. It is seen that simulation nos. 5–7 result in normal lock-in, but with increasing initial yaw rate, simulation no. 8 attains the stable design solution. Thus, for some set of initial conditions between those of simulation nos. 7 and 8 in Table 2 for case A, transient normal resonance is likely. Likewise, simulation nos. 13 and 14 for case A suggest transient normal resonance, while simulation nos. 7 and 8 for case B suggest transient reverse resonance.

Numerical simulation for the configuration of case A is shown in Figure 5 for an initial yaw rate of $\dot{\mu}_0 = 0 + 0{\cdot}726i$. There is a prolonged passage through normal resonance, but no amplification of the complex angle of attack is seen during this period. Figure 6 shows the numerical simulation for an initial yaw rate of $\dot{\mu}_0 = 0 + 0{\cdot}975i$ for the configuration of case B. The roll rate is seen to dither about the reverse resonance value for a considerable period of time before passing through normal resonance and going on to the design value. Once again, no yaw amplification is seen during transient reverse resonance, although an increase in complex angle of attack is evident around *time* = 110, when the roll rate is near the unstable normal resonance solution. Figures 5 and 6 seem to indicate that amplification of the trim angle of attack, as seen at lock-in in Figures 3 and 4, does not occur during transient resonance.

It must be noted that these initial yaw rates are only representative, and the possibility of transient resonance is not limited to these initial conditions. However it was noticed that

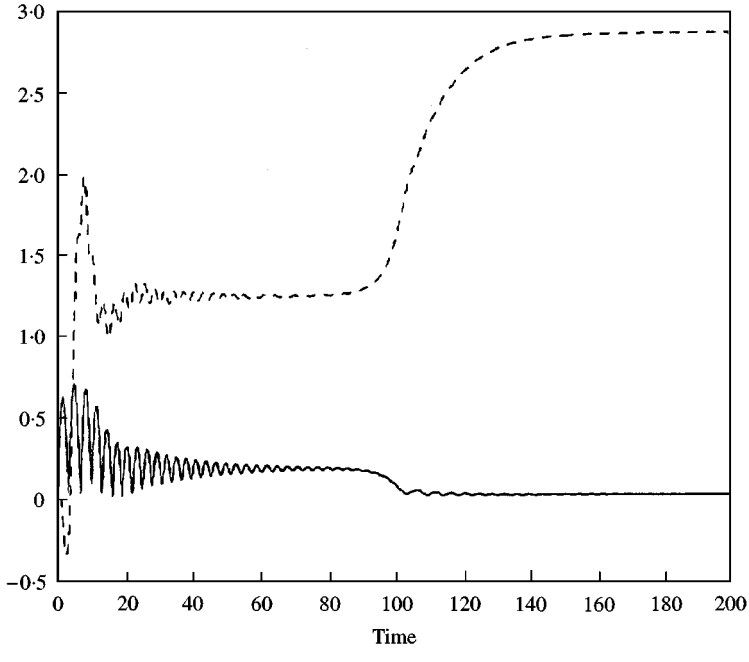

Figure 5. Variation of roll rate $\dot{\phi}$ (----), and magnitude of complex angle of attack $|\mu|$ (——) for $\dot{\mu}_0 = 0 + 0{\cdot}726i$, case A.

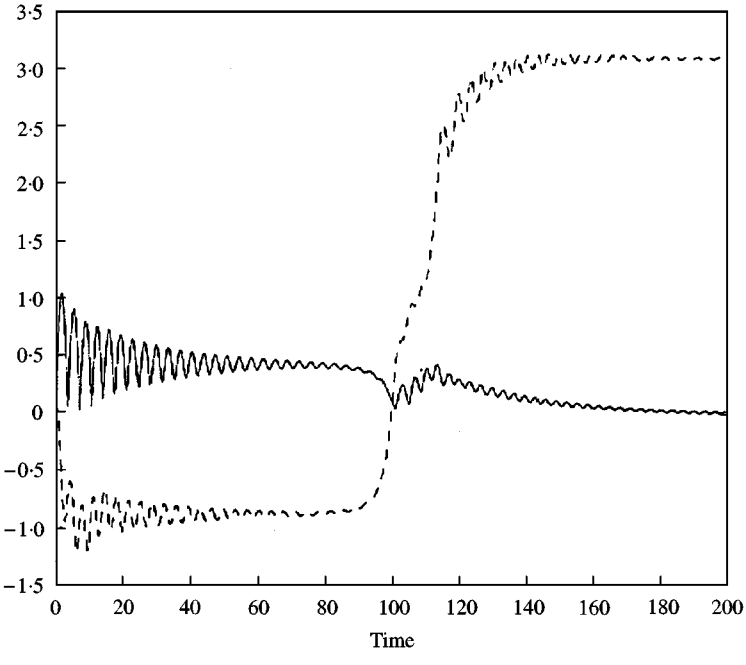

Figure 6. Variation of roll rate $\dot{\phi}$ (----), and magnitude of complex angle of attack $|\mu|$ (——) for $\dot{\mu}_0 = 0 + 0{\cdot}975i$, case B.

while transient normal resonance was quite common, transient reverse resonance was found to occur for a restricted set of initial yaw rates.

3.1. TRIM AMPLIFICATION

In order to evaluate the variation of the magnitude of complex angle of attack during transient resonance, numerical simulation of the configuration of case A is carried out for a different initial yaw rate, $\dot{\mu}_0 = 0 - 0{\cdot}192i$. The projectile is seen to experience transient normal resonance for this initial condition. The yaw amplification in this case is compared with the yaw for an ideal case of $G = 0$ with the same initial yaw rate. This comparison is shown in Figure 7 where the roll rate for the ideal projectile builds up smoothly to the design value of 3·0, whereas the projectile with center-of-mass offset shows prolonged transient resonance. A comparison of the magnitudes of the complex angle of attack in Figure 7 shows that while the yaw during transient resonance is larger than in the ideal case, there is no significant build-up. Further, the numerical simulation of transient resonance in Figure 7 is compared with that of a projectile with identical configuration but with a slightly different initial condition that leads to normal lock-in. This comparison is plotted in Figure 8 where the yaw response indicates a significant drop in yaw magnitude for the projectile in transient normal resonance ($time = 25$–100) as compared to the yaw for the projectile in normal lock-in. Thus, the evidence in Figures 7 and 8 indicates that transient resonance does not result in trim amplification unlike that noticed during lock-in.

The key to understanding this lack of trim amplification lies in noticing that the roll rate during transient resonance in Figure 8 does not match the lock-in roll rate. Referring to Table 1, case A, it is seen that the roll rate during transient resonance corresponds to the unstable solution paired with the stable normal resonance solution. The complex angle of

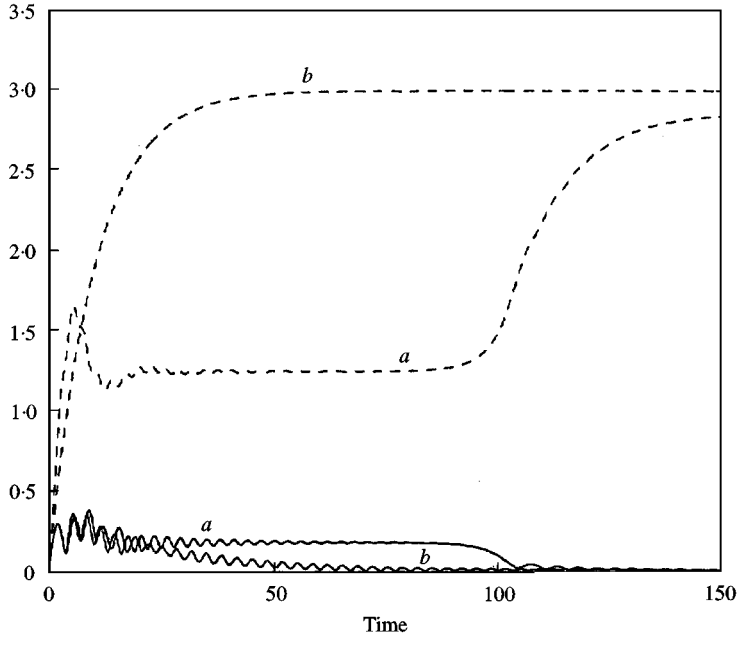

Figure 7. Variation of roll rate $\dot{\phi}$ (----) and magnitude of complex angle of attack $|\mu|$ (——) for $\dot{\mu}_0 = 0 - 0{\cdot}192i$, case A with (a) $G = 5$, and (b) $G = 0$.

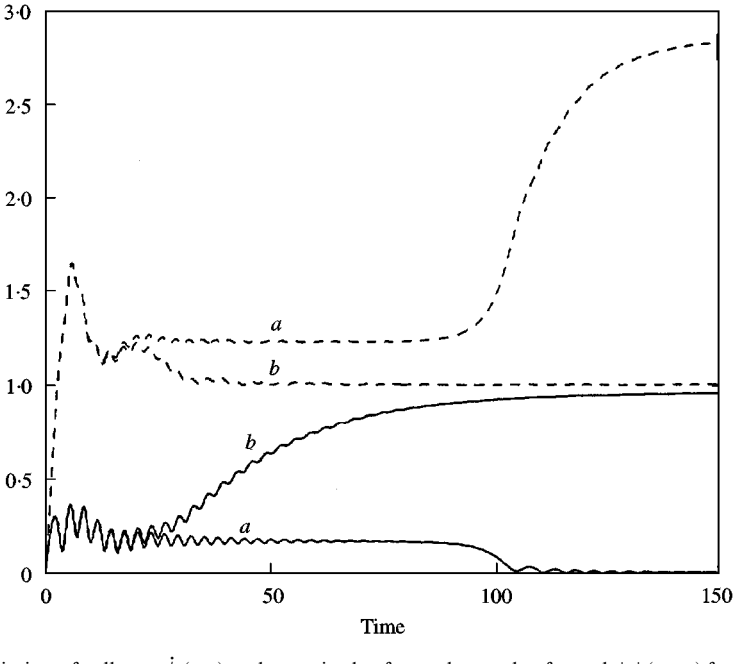

Figure 8. Variation of roll rate $\dot{\phi}$ (----) and magnitude of complex angle of attack $|\mu|$ (——) for case A with (a) $\dot{\mu}_0 = 0 - 0{\cdot}192i$, and (b) $\dot{\mu}_0 = 0 - 0{\cdot}2i$.

attack magnitude can be calculated to be 0·180 at the unstable solution as compared to 0·967 at the resonance solution. Thus, during transient resonance, the projectile temporarily locks in at the unstable equilibrium close to the resonance condition. As the yaw magnitudes associated with this unstable equilibrium are significantly smaller than those at

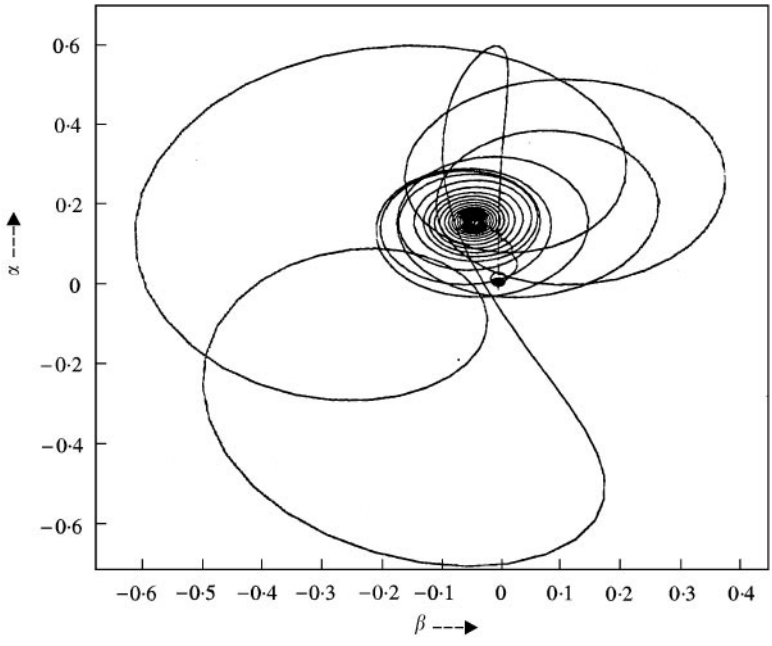

Figure 9. Trajectory in β–α plane for $\dot{\mu}_0 = 0 + 0{\cdot}726i$, case A.

resonance, trim amplification at transient resonance is limited. Nevertheless, the yaw magnitude at transient resonance is larger than that at the design solution (0·015 for case A in Table 1).

Observation of the roll rate during transient resonance for the simulations in Figures 5 and 6 confirms the above diagnosis. In each case, the roll rate during transient resonance matches the roll rate of the unstable equilibrium pair of the stable normal resonance solution. Further confirmation can be sought by plotting the trajectory for the simulations in Figures 5 and 6 in the β–α plane. The trajectory for passage through normal resonance in Figure 5, plotted in Figure 9, can be seen to encircle the unstable equilibrium point at $\dot{\phi} = 1{\cdot}241$ for case A in Table 1 for a while before converging towards the design yaw near the origin. Similarly, the trajectory for passage through reverse resonance, shown in Figure 10, oscillates about the unstable equilibrium point at $\dot{\phi} = -0{\cdot}882$ for case B in Table 1 before settling down at the design yaw near the origin. Thus, it can be concluded that a projectile in transient resonance temporarily locks in at an unstable equilibrium solution in the vicinity of the stable resonance solution. The resulting amplification of the trim angle during transient resonance is therefore much lower than that at lock-in. It can also be argued in support of this conclusion that if the projectile were to exhibit a roll rate and a complex angle of attack near that of the stable resonance solution, then it would most likely be within the basin of attraction of that stable equilibrium, and would therefore lock-in, rather than escape to the design solution.

4. BIFURCATION ANALYSIS

The above description of transient resonance also raises the possibility that a projectile with stable design solution and an unstable equilibrium at normal resonance may temporarily lock-in at resonance with large trim amplification before attaining the design

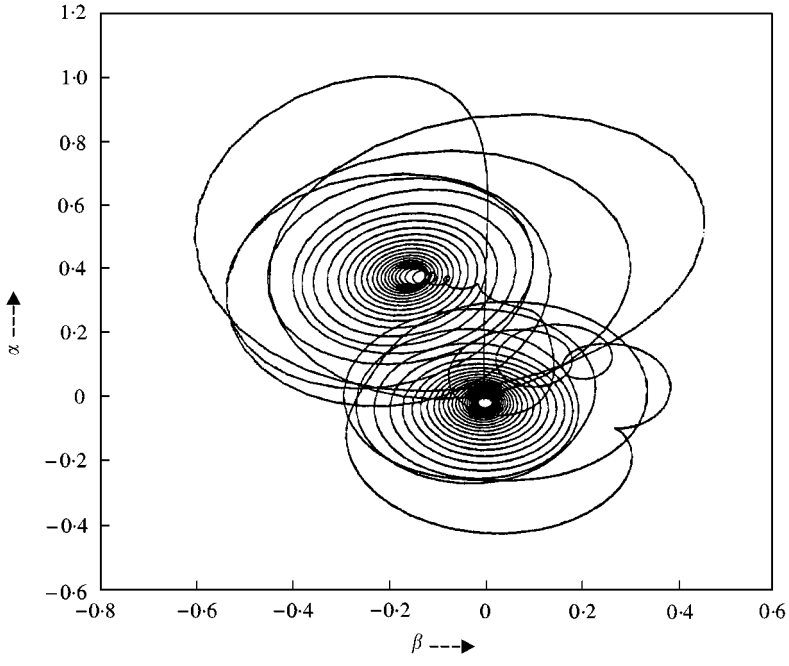

Figure 10. Trajectory in β–α plane for $\dot{\mu}_0 = 0 + 0{\cdot}975i$, case B.

steady state. A hint of this phenomenon is seen in Figure 6 where, after transient reverse resonance, the roll rate builds up to the design value through a pair of unstable equilibria at $\dot{\phi} = 0{\cdot}754$ and $0{\cdot}990$. As the roll rate passes through the unstable resonance solution at $\dot{\phi} = 0{\cdot}990$, the yaw magnitude in Figure 6 shows a notable increase. It is therefore of interest to explore the possibility of transient resonance with trim amplification in cases where the design solution is stable, whereas the resonance solution is unstable. Such cases are also of practical interest since long-time transient resonance of this nature could result in the failure of the projectile, while the stability analysis would indicate no stable lock-in.

From an inspection of equation (2), the two main parameters influencing the stability of the yaw dynamics are the yaw damping $\hat{H}$, and the trim asymmetry h. Consider the dynamics in case A, Table 1 where both the design and normal resonance solutions are stable. With varying h or $\hat{H}$, if the normal resonance solution goes unstable while the design solution still retains stability, then transient resonance with large yaw, as described above is likely. Also, the question of whether stable normal resonance persists when the parameters h and $\hat{H}$ are varied from their baseline values needs to be answered. To this end, bifurcation analysis of the equilibrium solutions in case A, Table 1 is carried out with one parameter, h or $\hat{H}$, varied while the other parameters are held fixed.

4.1. VARIATION OF h

The bifurcation diagram with trim asymmetry parameter h varied 50 per cent about its baseline value is plotted in Figure 11. The design solution is seen to lose stability with both increasing and decreasing h at Hopf bifurcations. The limit cycles expected to emerge at these Hopf bifurcations are not plotted in Figure 11 as their nature is strongly

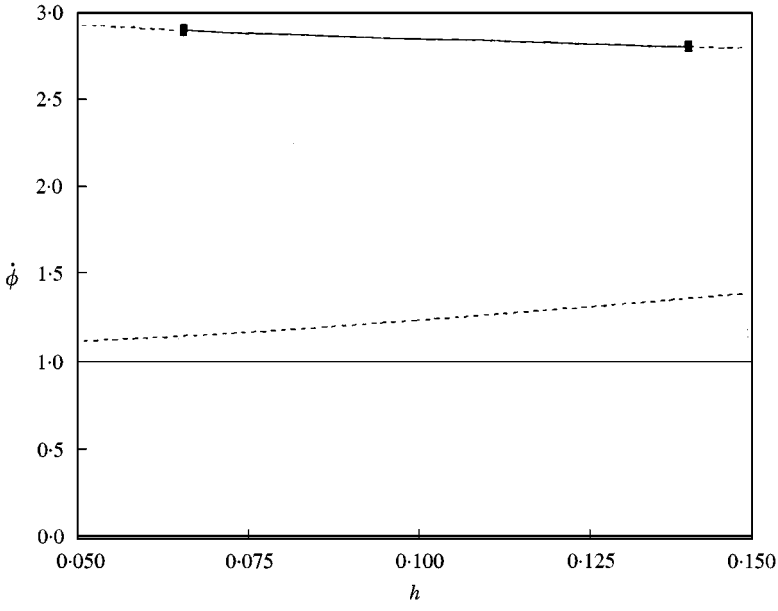

Figure 11. Equilibrium roll rates with varying h for case A, Table 1: ——, stable equilibria; ----, unstable equilibria: ■ ■, Hopf bifurcation.

dependent on non-linear terms in the yaw equation that have been neglected in the present formulation. The resonance solution is seen to remain stable along with its unstable equilibrium pair. The instability of the design solution with varying h is well-known and can be traced to the influence of the Magnus moment coefficient $Cm_{p\alpha}$ in $\hat{T}$ which is included in the definition of h. Traditionally, onset of this instability is given in terms of a gyroscopic stability factor s_g and a dynamic stability factor s_d, and is called Murphy's stability criterion [8, 17]. As the normal resonance solution continues to be stable while the design solution loses stability, transient normal resonance with large yaw is not likely to occur in this case.

4.2. VARIATION OF $\hat{H}$

The bifurcation diagram with yaw damping parameter $\hat{H}$ varied 50 per cent about its baseline value is plotted in Figure 12. The design solution is again seen to lose stability with both increasing and decreasing $\hat{H}$ at Hopf bifurcations. This instability is the same as that predicted by Murphy's criterion. Interestingly, the normal resonance solution also loses stability at a Hopf bifurcation with decreasing $\hat{H}$, but for a value of $\hat{H}$ less than that at the Hopf point of the design solution. Thus, there is no range of $\hat{H}$ with stable design and unstable normal resonance solution. Transient resonance with large trim angles is, therefore, not expected to be seen in this case either.

The instability of the normal resonance solution with decreasing $\hat{H}$ has not been previously predicted, although the possibility had been suggested in reference [6]. The Hopf bifurcation of the normal resonance solution is expected to result in catastrophic yaw limit cycles, provided the non-linear yawing moments, which have been neglected in the present formulation, are taken into account.

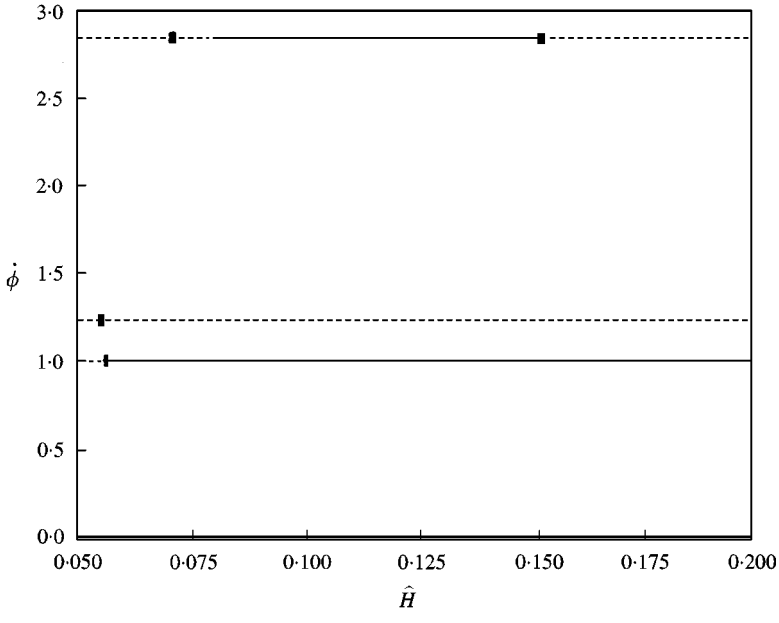

Figure 12. Equilibrium roll rates with varying $\hat{H}$ for case A, Table 1 ——, stable equilibria, ----, unstable equilibria; ■ ■, Hopf bifurcation.

5. CONCLUSIONS

The phenomenon of transient resonance in the passage-through-resonance problem of rolling finned projectiles with an offset center of mass has been studied. Bifurcation analysis of the equilibrium solutions reveals that stable normal and reverse resonance solutions are paired with an unstable equilibrium point. When the projectile locks in at stable normal or reverse resonance, a build-up in the complex angle of attack magnitude is seen. Similar yaw amplification is not observed during transient normal and reverse resonance. This is explained by noticing that the projectile in transient resonance temporarily locks in at the unstable equilibrium point paired with the stable resonance solution. Thus, the trim angle of attack during transient resonance is much smaller than that at lock-in. Bifurcation analysis is used to rule out transient resonance at unstable normal or reverse resonance, which could have resulted in significant yaw amplification.

REFERENCES

1. A. G. MIKHAIL 1998 *Journal of Spacecraft and Rockets* **35**, 287–295. Fin damage and mass offset for kinetic energy projectile spin/pitch lock-in.
2. E. J. MCSHANE, J. L. KELLEY and F. V. RENO 1953 *Exterior Ballistics*. Denver: University of Denver Press.
3. J. D. NICOLAIDES 1959 *Report* 59–17, *Institute of the Aeronautical Sciences*. Two nonlinear problems in the flight dynamics of modern ballistic missiles.
4. D. A. PRICE 1967 *Journal of Spacecraft and Rockets* **4**, 1516–1525. Sources, mechanisms, and control of roll resonance phenomena for sounding rockets.
5. C. H. MURPHY 1989 *Journal of Guidance, Control, and Dynamics* **12**, 771–776. Some special cases of spin-yaw lock-in.
6. N. ANANTHKRISHNAN and S. C. RAISINGHANI 1992 *Journal of Spacecraft and Rockets* **29**, 692–696. Steady and quasisteady resonant lock-in of finned projectiles.

7. N. ANANTHKRISHNAN and S. C. RAISINGHANI 1994 *Journal of the Institution of Engineers* (*India*) **74**, 37–43. Theory of resonant lock-in of rolling finned projectiles.
8. C. H. MURPHY 1981 *Journal of Guidance, Control, and Dynamics* **4**, 464–471. Symmetric missile dynamic instabilities.
9. D. H. PLATUS 1982 *Journal of Guidance, Control, and Dynamics* **5**, 4–16. Ballistic re-entry vehicle flight dynamics.
10. D. H. PLATUS 1994 *Journal of Guidance, Control, and Dynamics* **17**, 1012–1018. Missile and spacecraft coning instabilities.
11. F. J. BARBERA 1969 *Journal of Spacecraft and Rockets* **6**, 1279–1284. An analytical technique for studying the anomalous roll behavior of re-entry vehicles.
12. W. R. CHADWICK 1967 *Journal of Spacecraft and Rockets* **4**, 768–773. Flight dynamics of a bomb with cruciform tail.
13. E. J. DOEDEL, X. J. WANG and T. F. FAIRGRIEVE 1995 *Report AUTO*94: *California Institute of Technology*. Software for continuation and bifurcation problems in ordinary differential equations.
14. R. H. RAND, R. J. KINSEY and D. L. MINGORI 1993 *International Journal of Nonlinear Mechanics* **27**, 489–502. Dynamics of spinup through resonance.
15. A. SHARMA 1999 *B. Tech. Project Report, Department of Aerospace Engineering, Indian Institute of Technology, Bombay*. Passage through resonance of rolling finned missiles with center-of-mass offset.
16. S. H. STROGATZ 1994 *Nonlinear Dynamics and Chaos*. Reading, Massachusetts: Addison-Wesley.
17. Y. L. LING and K. W. HAN 1980 *Israel Journal of Technology* **18**, 65–69. Stability analysis of angular motion of rolling missiles.

APPENDIX A: NOMENCLATURE

C_D	drag force coefficient
C_{l_p}	spin-damping moment coefficient
$C_{M_{p\alpha}}$	Magnus moment coefficient
$C_{M_q} + C_{M_{\dot\alpha}}$	damping moment coefficient sum
C_{M_0}	asymmetry moment coefficient
C_{M_α}	static moment coefficient
C_{N_0}	asymmetry force coefficient
C_{N_α}	normal force coefficient
G	$(= -(1/2h)(\hat{r}_c\delta_{T_0}C_{N_\alpha})[C_{lp} + (I_x/ml^2)C_D]^{-1}[-(1-\sigma)/M]^{0\cdot5}$
H	$(= (\rho Sl/2m)[C_{N_\alpha} - C_D - (ml^2/I)(C_{M_q} + C_{M_{\dot\alpha}})])$
h	$(= (\hat{H} - \sigma\hat{T})/(1-\sigma))$
I	transverse moment of inertia
I_x	axial moment of inertia
K_p	$(= -(\rho Sl^3/2I_x)[C_{lp} + (I_x/ml^2)C_D]$
l	reference length, diam
M	$(= (\rho Sl^3/2I)C_{M\alpha}$
m	mass
$\hat{r_c}$	radial center of mass offset, calibers
S	reference area
s	$(= \int_0^t (u/l)\,\mathrm{d}t)$
T	$(\rho Sl/2m)[C_{N_\alpha} - C_D + (ml^2/I_x)C_{M_{p\alpha}}])$
t	time
t_1	$(= [-M/(1-\sigma)]^{0\cdot5}s)$
u	magnitude of the velocity
α, β	angle of attack and sideslip in missile-fixed axes
δ	absolute value of ξ
δ_{TR}	$(= -\delta_{T0}/h)$
δ_{T0}	$(= -C_{M_0}/C_{M_\alpha})$, magnitude of non-rolling trim
θ	orientation angle of ξ in missile-fixed axes
ξ	$(= \beta + \mathrm{i}\alpha = \delta\mathrm{e}^{\mathrm{i}\theta})$, complex angle of attack in the missile-fixed axes
ρ	air density
σ	I_x/I

μ	$(=\xi/\delta_{TR})$
ϕ_M	orientation angle of non-rolling trim
ϕ	roll angle
$\dot{\phi}_s$	design roll rate

Superscripts

$(\bar{\ })$	complex conjugate
$(\hat{\ })$	$[-(1-\sigma)/M]^{0.5}(\ )$
$(\dot{\ })$	$\mathrm{d}(\ )/\mathrm{d}t_1$

Subscripts

e	equilibrium value